

# CHARACTERIZING SUPERSONIC GAS JET-BASED BEAM PROFILE MONITORS

H. Zhang, V. Tzoganis<sup>1</sup>, A. Jeff<sup>2</sup>, A. Alexandrova and C.P. Welsch, Cockcroft Institute and the University of Liverpool, UK

<sup>1</sup>also at RIKEN Nishina Center, Japan

<sup>2</sup>also at CERN, 1211 Geneve 23, Switzerland

## Abstract

The next generation of high power, high intensity accelerators requires non-invasive diagnostics, particularly beam profile monitors. Residual gas-based diagnostics such as ionization beam profile or beam induced fluorescence monitors have been used to replace commonly used scintillating screens. At the Cockcroft Institute an alternative technique using a supersonic gas jet, shaped into a 45° curtain screen, was developed. It has already demonstrated its superior performance in terms of resolution and signal-to-noise ratio in comparison with residual gas monitors in experimental studies. The performance of this type of monitor depends on the achievable jet homogeneity and quality. Using a movable vacuum gauge as a scanner, the dynamic characteristics of the jet are studied. In this paper we also give an analysis of the resolution for this monitor in detail from the theory and ion drift simulation.

in the reaction rate and hence reduces the acquisition time. Furthermore, this scheme allows the measurement in two dimensions with a single unit. We have previously reported on the development and first tests with such a monitor at the Cockcroft Institute [5, 6]. We successfully measured beam sizes as small as 0.5 mm in two dimensions. In this paper, we briefly describe the whole setup and its working principle, before we discuss the resolution of this method in detail by comparing simulations into the ions drift process with experimental data.

## INTRODUCTION

The development of high energy and high intensity accelerators with high beam power limit the usage of most diagnostic devices, in particular when it comes to beam profile measurement. Different gas-based diagnostics has been successfully applied to measure the beam profile non-invasively. This included Ionization Profile Monitors (IPM) [1] and Beam Induced Fluorescence (BIF) monitors [2]. However, both of them require rather long signal acquisition times due to the ultra-high vacuum and low gas density, and can only measure the beam profile in one dimension with a single unit. More recently, supersonic gas jets [3, 4] were used to increase the local gas density which leads to an increase

## WORK PRINCIPLE AND MEASUREMENT

The schematic of the supersonic gas jet beam profile monitor is shown in Fig. 1. In a first nozzle chamber, a high pressure gas flows through a 30 μm nozzle and expands freely into vacuum. It reaches a supersonic speed due to a significant pressure ratio of about 10<sup>6</sup>. Before reaching the Barrel shock disk the flow is extracted by the first 180 μm conical skimmer and becomes a molecular flow. Further collimation is achieved by a second 400 μm conical skimmer and the final shape of the flow is then collimated to a rectangular curtain with a 45 degree orientation by a third skimmer of a 4\*0.4 mm<sup>2</sup> size. A laser system [7] was used to align the nozzle and the skimmers. An additional moveable gauge [8] was installed into the first dumping chamber for in-detail characterization of the jet. Turbo-molecular pumps backed with scroll pumps are used to achieve the required ultra-high vacuum environment [9] in each chamber. The angled flange in the last dumping chamber is required for reducing the back flow.

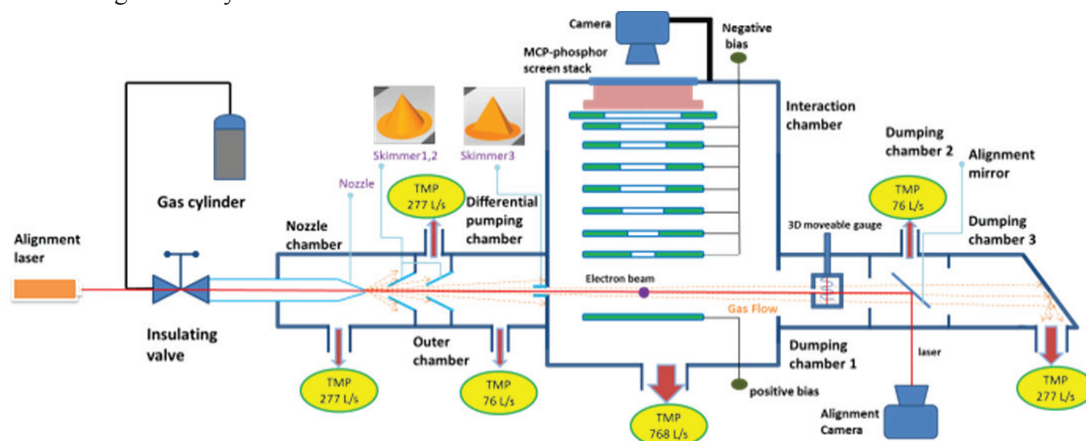


Figure 1: Schematic of the supersonic gas jet beam profile monitor.

A 3.5 keV electron beam with a 1  $\mu$ A current was used in the setup. It interacts with the supersonic gas jet and causes ionization. The generated ions are then accelerated by means of an external electric field and collected by a macro-channel-plate (MCP)-phosphor screen stack. The light emitted from the phosphor screen represents the distribution of the ions and hence the distribution of the initial electron beam. More details about the functioning principle can be found in [5, 6, 8]. One example of a measurement done at the Cockcroft Institute is shown in Fig. 2a. This shows an image from both, the gas jet and the residual gas. A data fit along the region of interest (ROI) indicated in the figure yields a size of  $\sigma_{x\_jet} = 0.54$  mm,  $\sigma_{y\_jet} = 0.56$  mm for the gas jet image and  $\sigma_{x\_res} = 1.34$  mm for the residual gas image. The separation of both images along the x-axis is  $d = 2.63$  mm.

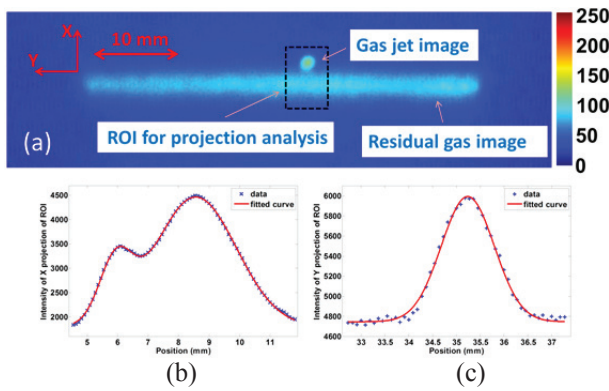


Figure 2: (a) Images of the electron beam from both gas jet (smaller size third skimmer) and residual gas; Gaussian fit for ROI in (b) x-axis and (c) y-axis.

### RESOLUTION

The resolution of this monitor can be influenced by many factors such as the resolution of the camera and the MCP, image broadening caused by the gas jet screen thickness and homogeneity, thermal spread of the generated ions, space charge of the primary beam and the external field. For the specific setup, the camera resolution is given by the size of one pixel which is  $\sigma_{CCD} = 90 \mu$ m. The MCP has two plates stacked in a chevron configuration, and its resolution is estimated as  $\sigma_{MCP} = 80 \mu$ m. The gas jet thickness only affects the resolution along one axis. Previous measurements [5] gave an estimate of the jet thickness of around  $\sigma_{jet} = 0.28$  mm. Since the electron beam current is low effects from space charge can be ignored. We simulated the thermal spread process under the action from an external field in WARP [10] using the same voltage setting used for the measurement shown in Fig. 2. Initially, a round Gaussian  $N_2^+$  beam was created at the interaction point assuming  $10^6$  particles. It was further assumed that the  $N_2^+$  ions have the same velocity spread as the  $N_2$  gas jet, the temperature of which is 10 K. The initial rms beam size was assumed to be 0.50 mm. Figure 3 shows the potential of the imaging electric field. The equipotential lines near the MCP are denser and more curved which indicates a large electric field in the z-

direction and also a presence of a radial component. In such an external field, the drift time is 3.455  $\mu$ s.

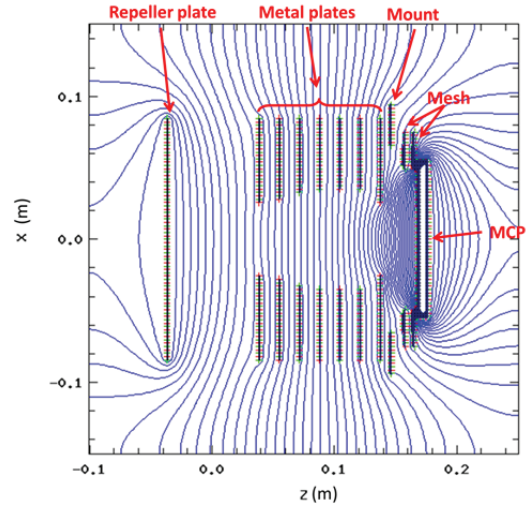


Figure 3: Electrostatic potential in z-x plane.

Figure 4 shows the beam size change during the drift process. When compared with Fig. 3, the radial component of the external field between the repeller plate and the first metal plate is insignificant, as thermal spread will dominate the drift process. Thus, as indicated in Fig. 4 between  $z = 0.0$  m and 0.04 m, the slope of the beam size growth is quite large. After entering the metal plates at  $z = 0.04$ -0.12 m, the focusing field is moderate and reduces the transverse thermal velocity. Therefore, the growth in beam size decreases. In the area between the last metal plate and the MCP, where there is a rapid growth of the potential, the radial component of the field is large enough to provide a focusing that is larger than the thermal spread. As a result, the beam size decreases. The final size of the beam is reduced to 0.51 mm due to a combined effect of the thermal spread and the external focusing field.

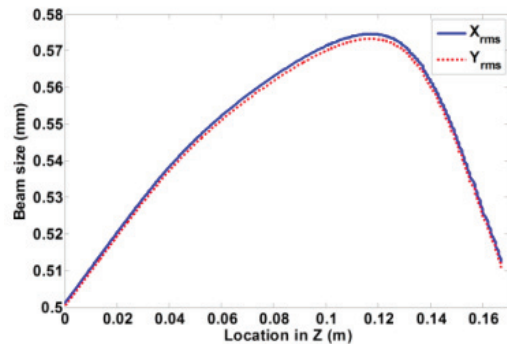


Figure 4: The change of ion beam size when propagating to the MCP under the action of an external field.

To further investigate these effects, we scanned the initial rms beam size between 0.2 mm to 1.7 mm, and meanwhile kept the total ion number the same. The measured beam size is shown in Fig. 5. Since the external field is radially symmetric, the external focusing field magnifies or de-magnifies the real beam size. This data can be fitted with the following equation:

$$\sigma_{measured} = \sqrt{M^2 \cdot \sigma_{real}^2 + \sigma_{thermal}^2} \quad (1)$$

where  $M$  represents the magnification factor of the external field and  $\sigma_{thermal}$  is the contribution from the thermal spread. The fitted curve is also shown in Fig. 5 and yields  $M = 0.97$  and  $\sigma_{thermal} = 0.17$  mm. Note that the magnification factor is directly related to the setting of the external field. In simulations, a clear change of this factor for different voltage setting was observed, especially the transverse component of the field and the drift time can be controlled by the longitudinal component. This can be optimized by using different voltage settings which can be done numerically. The thermal spread is related to the initial temperature of the generated ions and also to the drift time. Lower gas temperature and a fast drift time both reduce the thermal spread. Considering these two factors as well as the jet thickness, and including the uncertainty from camera and MCP resolution, the real beam size is  $\sigma_{x, real} = 0.53 \pm 0.12$  mm,  $\sigma_{y, real} = 0.47 \pm 0.12$  mm.

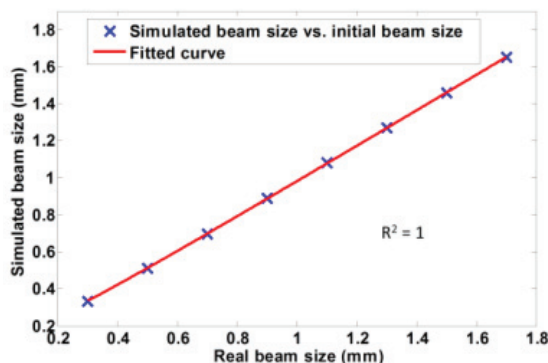


Figure 5: Simulated beam sizes after drift process as a function of initial beam size.

The ions from the residual gas can be simulated at room temperature, 300 K. This corresponds to a higher initial thermal spread. In simulations, the jet thickness can be added via the initial rms size along the y-axis in quadrature for the gas jet. For the residual gas operation mode, the thickness can be regarded as infinite, but it is limited by the geometry of the collecting plates. Moreover, ions from the gas jet will also hold an initial mean velocity along the jet flow direction and its magnitude can be estimated from the separation of both images in x-direction and the required drift time. This mean velocity was scanned in simulations and a velocity of 865 m/s was found to match the measured distance of 2.63 mm. From [11], the velocity of the gas jet can be calculated by Eq. 2:

$$v_{jet} = \sqrt{\frac{2\gamma kT_0}{\gamma-1 m}} \quad (2)$$

where  $k$  is a Boltzmann constant,  $\gamma$  is the heat capacity ratio, and  $T_0$  is the stagnation temperature (usually room temperature of 300 K). For molecular nitrogen,  $\gamma = 1.4$

and thus the theoretical jet velocity is 789 m/s. The difference between those two velocity values, one obtained in the experiment and the other one from theory is possibly caused by the accuracy of the measurement of the separation in the experiment. Other factors such as how nitrogen molecules differ from an ideal gas might also contribute.

In order to obtain an independent measurement of the velocity and density of the gas jet, a non-invasive and compact laser diode-based sensor is under development for usage in the gas-jet set-up [12, 13]. It is based on the scattering of the light on a moving target and exploitation of the Doppler shift for measurement of velocity. The sensor is based on the non-linear self-mixing effect inside a laser cavity, is very sensitive whilst not requiring a significant setup in itself.

The Fig. 6 below shows an example of a simulated result of an ion beam drifting towards the MCP with an initial beam size of  $0.53 \times 0.47$  mm<sup>2</sup>. It also shows a larger image broadening in the residual gas image than in the gas jet image. The rms size measured from the simulation data is  $\sigma_{x, jet} = 0.54$  mm,  $\sigma_{y, jet} = 0.60$  mm for the gas jet image and  $\sigma_{x, res} = 1.06$  mm for the residual gas image. The separation of both images along the x direction is 2.62 mm. These numbers agree well with the measured data.

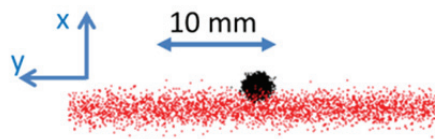


Figure 6: Simulated beam image at the location of the micro channel plate.

## CONCLUSION

In this paper, we reviewed recent development of a supersonic gas jet beam profile monitor in Cockcroft Institute. This diagnostic is non-invasive and can be used with essentially any primary beam. Based on measurements collected over the past two years, we have provided a detailed analysis of the resolution of the current setup. On the basis of the measured separation of two images, we estimated the gas jet velocity. Moreover, comprehensive simulations were performed to study the image broadening as a function of jet thickness, external fields and thermal drift processes. The results agree well with the experimental data.

## ACKNOWLEDGMENTS

This work was supported by the Helmholtz Association under contract VH-NG-328, the EU under grant agreement no 215080 and the STFC Cockcroft core grant No. ST/G008248/1.

## REFERENCES

- [1] J. Mießner, et al., *NIMA*, vol. 635, no. 1, pp. S104–S107, 2011.
- [2] F. Becker et al., *Proceedings of BIW2008*, Tahoe City, CA, USA, pp. TUPTPF054, 2008.
- [3] Y. Hashimoto, et al., *NIMA*, vol. 527, no. 3, pp. 289–300, 2004.
- [4] T. Tsang et al., *Rev. of Sci. Instr.*, vol. 79, no. 10, pp. 105103, 2008.
- [5] V. Tzoganis and C. P. Welsch, *Appl. Phys. Lett.*, vol. 104, no. 20, 2014.
- [6] H. Zhang, et al., *Proceedings of IPAC2015*, Richmond, VA, USA, pp. MOPWI006, 2015.
- [7] V. Tzoganis, et. al, *Proceedings of IBIC2013*, London, UK, pp. WEPF01, 2013.
- [8] H. Zhang, et al., *Proceedings of IBIC2015*, Melbourne, Australia, pp. TUPB075, 2015.
- [9] V. Tzoganis, et al., *Vacuum*, vol. 109, pp. 417–424, 2014.
- [10] A. Friedman, et al., *IEEE Trans. Plasma Sci.*, vol. 42, no. 5, pp. 1321–1334, 2014.
- [11] H. Pauly, ‘Atom, Molecule, and Cluster Beams I’, Taylor & Francis, Berlin, 2000
- [12] A. S. Alexandrova et al., *Opt. Eng.*, vol.54 no. 3, pp 034104, 2015.
- [13] A. S. Alexandrova et al., *NIMA*, ISSN 0168-9002, 2016.